Characteristics and Performances of a 100-W Hall Thruster for Microspacecraft

Stéphane Mazouffre and Lou Grimaud

Abstract— **In this paper, we examine the characteristics of the ISCT100 thruster, a miniature xenon-fueled 100-W permanent magnet Hall thruster (HT) suited for microspacecraft propulsion. The impact of the thruster design upon discharge behavior, ion beam properties, and performances is examined as for two discharge channel geometries as well as two values of the magnetic field strength. Thrust, specific impulse, and efficiency obtained between 50 and 200 W are compared with the ones of other low-power HTs.**

Index Terms— **Hall thruster (HT), low power, microspacecraft, performances.**

I. Introduction

OVER the last several decades, electronic and mechanical devices have drastically gained in terms of size, performance, and reliability while the cost continuously decreased. Among other things, those miniaturization processes and cost reductions have led to the emergence of small satellites able to accomplish most of tasks so far assigned to large-size and heavy satellites [1]. The observed trend on the satellite market should certainly accelerate as, in addition to the swift development of miniature platforms, small dedicated launchers will soon be available.

The mass is a relevant and useful criterion for the categorization of spacecraft as it has a direct link to cost. Here, we will use a classification in which the term "small spacecraft" covers spacecraft with masses below 500 kg. Four distinct groups are commonly considered as follows.

1) Minispacecraft: masses in 100–500 kg range.
2) Microspacecraft: masses in 10–100 kg range.
3) Nanospacecraft: masses in 1–10 kg range.
4) Picospacecraft: masses <1 kg.

Note that CubeSats fit into the second and third groups. In this paper, we solely focus on microspacecraft as they represent a good option in terms of operational capabilities-to-cost ratio against heavy satellites. Microsatellites are well-suited for various types of missions, such as Earth observation, communication, remote sensing, and science, with both civilian and military applications. As a matter of fact, they offer substantial advantages compared with heavy platforms: simplicity, low cost, flexibility, and turnover rate.

The ability to achieve a large variety of missions with microspacecraft requires, however, the use of an appropriate propulsion system. Although the last decade has seen significant advances in the miniaturization of propulsion units [2]–[4], satellite designers still lack high-efficiency space qualified devices that can cover a broad range of operating conditions. Electric propulsion is a suitable technology for microspacecraft as it offers a low propellant consumption, hence a low mass, long service life, large total impulse, and flexibility [5]. There are two distinct strategies to construct an efficient electrical micropropulsion system. The first one involves the development of new technologies. Examples of thruster that fall into this category are solid-propellant vacuum arc thrusters [6], liquid-propellant field emission electric propulsion devices [7], [8], liquid-propellant electrospray thrusters [9] and gaseous-propellant electron cyclotron resonant thrusters [10]. The second approach consists in the miniaturization of existing technologies with flight heritage. This category includes, inter alia, gridded ion engines [11]–[14] and Hall thrusters (HTs) [15], [16]. HTs, in addition to being simple and robust, deliver a large thrust-to-power ratio compared with ion engines with a specific impulse high enough to warrant substantial propellant mass saving [5]. Low-power HTs, therefore, appear as a good candidate as propulsion unit for microspacecraft. This paper deals with a xenon-fueled permanent magnet 100 W-class HT. First, the thruster architecture is described. Second, the plasma discharge as well as ion beam characteristics are reported for several configurations. Finally, thrust and performance level are given and compared with the ones of similar HTs.

II. Hall Thruster

A. Operation Principle

An HT is an electrical propulsion device for spacecraft that uses a plasma discharge with magnetized electrons to ionize and accelerate a propellant gas [5], [11], [15], [16]. The operation principle of a HT relies upon a magnetic barrier and a low-pressure dc discharge generated between a hot cathode and an anode in such a way that a crossed electric and magnetic field discharge is created. The anode is located at the upstream end of a coaxial annular dielectric channel that confines the discharge. A large fraction of the electrons emitted by the thermionic cathode that is placed outside the channel flows downstream to neutralize the ion

Manuscript received October 20, 2017; revised December 15, 2017; accepted December 15, 2017. Date of publication January 17, 2018; date of current version February 9, 2018. The work of L. Grimaud was supported by the CNES–Région Centre Ph.D. Grant. The review of this paper was arranged by Senior Editor S. J. Gitomer. *(Corresponding author: Stéphane Mazouffre.)*

The authors are with the Electric Propulsion Team, CNRS–Institut de Combustion, Aérothermique, Réactivité et Environnement Laboratory, 45071 Orléans, France (e-mail: stephane.mazouffre@cnrs-orleans.fr; lou.grimaud@cnrs-orleans.fr).

Color versions of one or more of the figures in this paper are available online at http://ieeexplore.ieee.org.

Digital Object Identifier 10.1109/TPS.2017.2786402

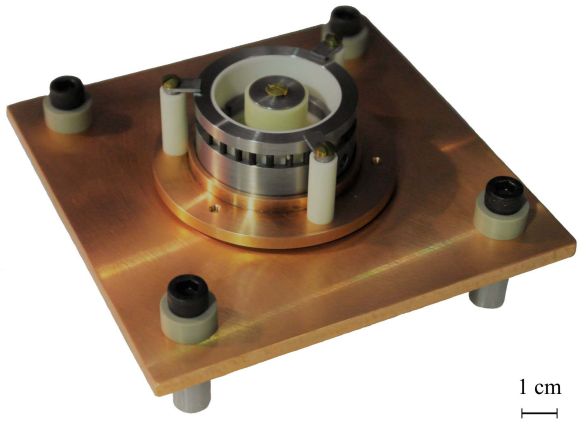

Fig. 1. Photograph of the 100-W-class permanent magnet ISCT100 HT developed at ICARE. The external cathode is not shown.

beam. The remaining part travels toward the anode to maintain the plasma discharge. The propellant gas, typically xenon, is introduced at the back of the channel either through the anode or using a dedicated injection system. Magnetizing coils or permanent magnets, incorporated into a magnetic circuit made of iron or iron–cobalt alloys, provide a radially directed magnetic field of which the strength is maximum in the vicinity of the channel exhaust. The magnetic field is chosen to be strong enough to make the electron Larmor radius much smaller than the discharge chamber characteristic dimensions, but weak enough not to affect ion trajectories. The electric potential drop is mostly concentrated in the final section of the channel owing to the low axial mobility of electrons that are magnetically confined in this restricted area. The electric field, which extends between the interior and the exterior of the channel, governs the propellant atoms ionization and the ion acceleration, namely, the thrust and the specific impulse. The combination of the radial magnetic field with the axial electric field generates an $\mathbf{E} \times \mathbf{B}$ electron drift in the azimuthal direction, the so-called Hall current. The latter is responsible for the very efficient ionization of neutral atoms inside the channel.

HTs provide a moderate specific impulse level <2000 s in contrast with gridded ion engines, but the thrust-to-power ratio is typically 60 mN/kW and the thrust density is above 30 N/m^2 as there is no space-charge limitation on the ion current. In comparison, the two quantities amount to 30 mN/kW and about 5 N/m^2, respectively, for ion engines. The thrust efficiency is about 50% for moderate power HTs (~1 kW), but it is in excess of 60% for high-power devices, see [17] and references herein.

B. Low-Power Devices

A great challenge in developing low-power HTs is to achieve high thrust efficiency while keeping a long lifetime. Operation at low power requires a decrease in size in order to maintain a sufficient ionization rate. Yet miniature HTs exhibit a large surface-to-volume ratio, which translates into large power losses, large channel wall erosion rate, and overheating of magnetic circuit components. Many works have nevertheless been performed all around the world to develop, characterize, and qualify 200-W-class HTs, which are well-adapted for drag compensation, trajectory changes, attitude control, and end-of-life deorbiting of 100–200 kg satellites in Earth orbit. Such thrusters typically deliver 10 mN of thrust with an efficiency around 40% despite small dimensions. Currently, the most advanced devices are, to the best of our knowledge, the BHT200 American HT [18], the SPT30 and Plas-40 Russian HTs [19], [20], the CAM200 Israeli HT [21], the HT100 Italian HT [22], the KAIST Korean HT [23], and the ISCT200 French HT [24]. The inclined reader can find additional information about low-power annular HTs in [24] and [25] and references herein.

Very few relevant and reliable studies have been carried out so far on HTs with input power below 200 W. In this paper, the design of a 100-W-class permanent magnet HT operating with xenon is described and performances along with ion beam property measurements are given and discussed. On a fundamental viewpoint, this paper furnishes low-power data to verify the validity of established scaling laws and to test computer simulations. On a more technological standpoint, this paper is a necessary step to develop a robust low-cost EP system based on a 100-W HT able to produce a few mN of thrust at high specific impulse with a reasonable efficiency. Such a propulsion unit would be of interest for maneuvering large CubeSats and 50–100 kg satellites.

C. 100-W Architecture

The Institut de Combustion, Aérothermique, Réactivité et Environnement (ICARE) small customizable thruster 100, or ISCT100 in short, is a 100-W-class HT of which the architecture derives from the 200 W input power ISCT200 thruster series [24], [26]. The annular channel walls of the ISCT100 are made of BN-SiO_2 ceramic. The channel width h can easily be modified while keeping the mean diameter d unchanged by means of various sets of ceramic rings. Works on scaling laws and HT design have shown that a large h leads to higher propellant utilization, thrust, and anode efficiency [26]. Higher performance level originates in the decrease of wall losses due to a more favorable surface-to-volume ratio. In this paper, two geometrical configurations have been used, the so-called S_0 and $2S_0$ configurations, by installing two sets of ceramic rings, such that the channel cross-sectional area is either S_0 or two times S_0, wherein $S_0 = \pi h_0 \, d_0$ corresponds to the standard value of the well-known Russian SPT100. The channel length l is selected to maintain neutral density in the order of the critical density, which ensures a high-ionization degree [27]. The channel has also to be long enough to allow the ionization region to fully expand. The magnetic field is generated by way of small cylindrical samarium–cobalt (SmCo) magnets brought together inside rings located on either side of the channel walls. SmCo magnets exhibit a high Curie point, which allows operation at relatively high temperature. Magnets are attractive in terms of power, volume, and mass saving. But, contrary to magnetizing coils, instant adjustment of magnetic field magnitude and topology cannot be achieved. The choice between the two technological options depends on mission profile and constraints. A soft iron magnetic circuit with a back gap permits to drive the

magnetic flux for obtaining the desired topology. No magnetic screen is used. The magnetic field strength can be varied by simply changing the number of magnets. In the case of the ISCT100, the **B** field has a classical bell-shape distribution along the channel centerline with the highest intensity at the channel exit plane. Two magnetic field maximum magnitudes have been tested in this paper, namely, B_0 and $2B_0$ with $2B_0 = 2 \times B_0$. The field amplitude must be chosen according to three criteria. First, electrons must be magnetized to generate the $\mathbf{E} \times \mathbf{B}$ electron azimuthal drift. Second, the electron gyroperiod in the magnetic barrier must be much shorter than the time between two consecutive electron–atom collisions to minimize electron diffusion losses. Finally, the magnetic confinement of the electron fluid must enable a long residence time in order to maximize the ionization yield. The propellant gas—xenon in this paper—is injected homogeneously inside the channel using a mullite ring, high porosity ceramics, instead of a classical metal hollow gas injector. The mullite element is placed behind the channel back plate. A narrow annular gap in the back plate allows diffusion of the gas. The anode is a wide stainless steel ring placed at the back of the channel against the internal surface of the outer dielectric wall. A central copper heat drain is employed to evacuate heat toward a radiator placed behind the thruster body. During operation, the thruster body is floating. A heated hollow cathode with a disk-shaped LaB_6 emitter was used to generate the electron current needed for discharge balance and ion beam neutralization [28]. The cathode is located outside the channel with its orifice in the vertical plane that contains the channel outlet. The cathode is electrically connected to the thruster anode and floating. High-purity xenon was used as the propellant gas for both the thruster discharge and the cathode discharge. The cathode has been operated with a constant xenon mass flow rate of 0.2 mg/s.

A photograph of the ISCT100 HT is shown in Fig. 1 without the external cathode. The visible copper ring is the radiator. The square copper plate area corresponds to a 1-U CubeSat cross-sectional area, i.e., 100 cm^2. The total outside volume and mass of the ISCT100 thruster are 115 cm^3 and 360 g, respectively. The oversized copper heat sink represent 230 g of this total mass and could easily be made twice as light if any mass or thermal optimization were conducted. Fig. 2 shows the ISCT100 HT in $2S_0$ B_0 configuration firing with xenon at 100-W input power.

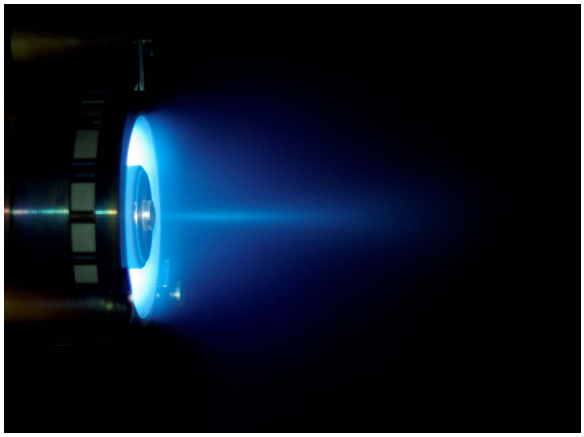

Fig. 2. ISCT100 HT in $2S_0$ B_0 configuration firing with xenon at 100-W input power. The residual gas pressure in the vacuum chamber is 4×10^{-5} mbar.

III. Results

A. Discharge Envelope

The four different configurations were tested first in the NExET vacuum chamber to assess their operating envelope and stability. The NExET chamber is a $\varnothing 0.8 \times 1.8$ m stainless steel cylinder with grounded walls fit with both a cryogenic and turbomolecular pumping system. During measurements the background pressure was between 1 and 4×10^{-5} mBar depending on the mass flow rate.

Fig. 3 shows the map of tested operating points. The shaded areas cover 90% of the discharge current oscillations. All the configurations were tested from extinction voltage up to either 200-W discharge power, the apparition of hot spots in the discharge channel or spontaneous shutdown (whichever came first). Spontaneous shutdown seemed to be mainly caused by very high oscillations. Before even looking at current profile it is interesting to note that thruster startup was made considerably harder as the magnetic field was increased and the channel width narrowed. The S_0 $2B_0$ case required high voltage ($\sim$400 V) and high mass flow ($\sim$1 mg/s) in order to ignite it. Identical trend was observed with the ISCT200 HT in previous works [26].

Out of all those configurations, only the $2S_0$ $2B_0$ one is stable over a large number of operating points, see Fig. 3(d). Both $2B_0$ configurations have a discharge envelope resembling a classical HT, such as the SPT100 [29]. In the $2S_0$ $2B_0$ case, the oscillations are restrained to around 10% of the mean discharge current for most points. There is a steady moderate increase of discharge current as the voltage increase for a fixed mass flow rate above 150 V. The oscillations also slightly increase with voltage but the strong oscillation regime sometime seen at higher voltage is not observed. As can be seen in Fig. 3(b), the S_0 $2B_0$ case displays a local maximum of the discharge current between 150 and 200 V before settling into a nearly constant mean discharge current regime. As the voltage is increased, a high oscillation "breathing mode"-like regime appears, with the dominant frequency in the 30–35 kHz range. This regime was only seen above 350 V for the SPT100 [29]. In the case of the ISCT100 with the S_0 $2B_0$ configuration, it appears from 225 V.

B. Plume Divergence and Characteristics

1) Plume Current Density Profiles: For all configurations an ion current density angular profile was acquired across the plume. Those profiles were acquired with a 5.6-mm-diameter molybdenum planar probe fitted with a guard ring. The probe is swept in front of the thruster on a 180° hemisphere with a 35-cm radius. The angular profiles measured for each configuration at three different operating conditions are displayed in Fig. 4.

The S_0 B_0 case clearly shows an unfocused beam with a significant portion of the ion current present at high angles.

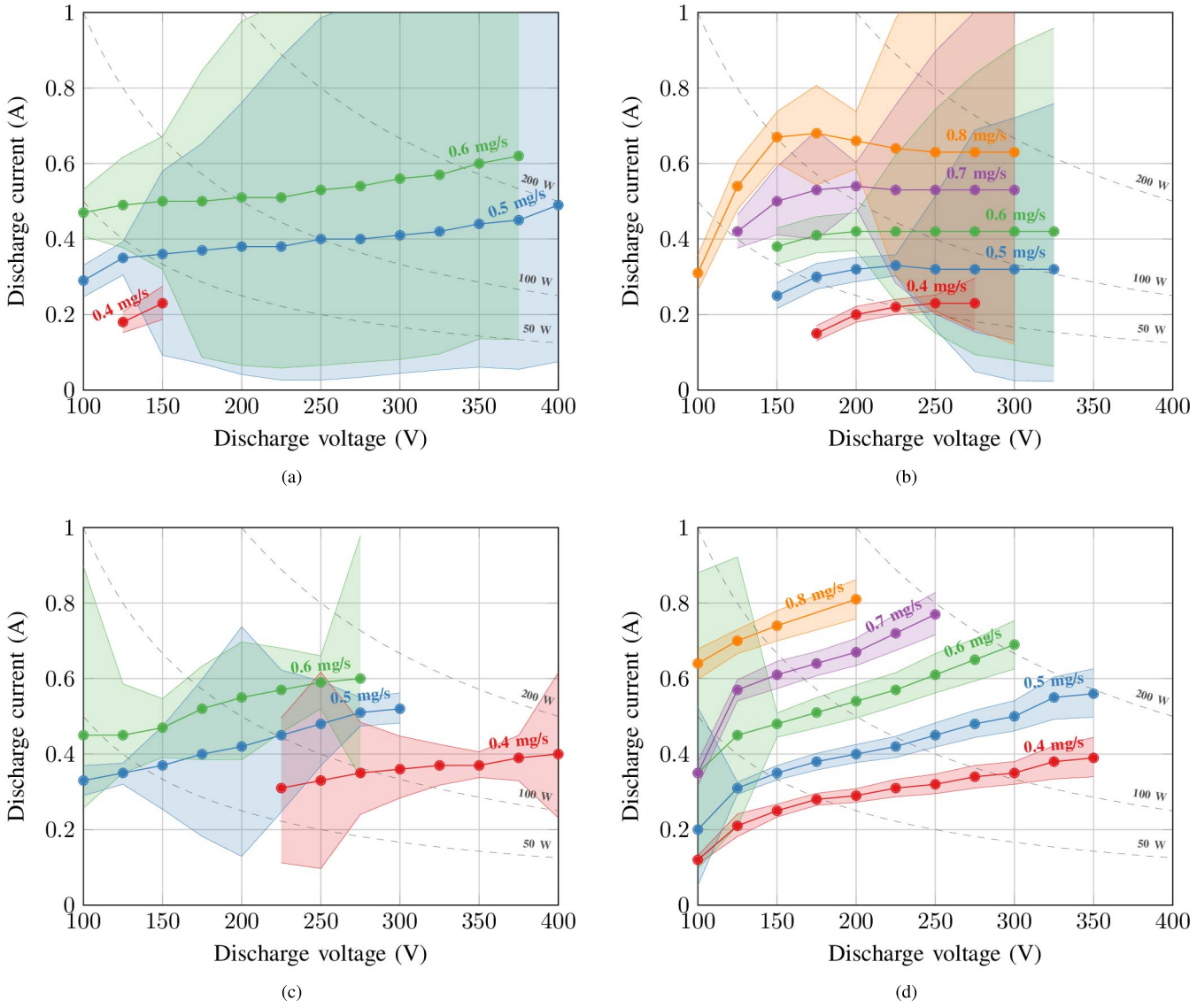

Fig. 3. ISCT100 HT discharge current as a function of anode mass flow rate and discharge voltage for different configurations. (a) S_0 B_0. (b) S_0 $2B_0$. (c) $2S_0$ B_0. (d) $2S_0$ $2B_0$.

The S_0 $2B_0$ only has this Gaussian shaped current density distribution at 300 V and 0.5 mg/s. For both the cases, it is correlated with very high current oscillation regimes. For the angular profiles corresponding to more stable operating points, the two peaks, coming from the two opposite sides of the discharge channel, are visible. The resolution of those two peaks is characteristic of a well-focused ion beam.

2) Plume Characteristics: From the angular distribution of the ion current density, it is possible to calculate the total ion current by integrating the distribution over the whole hemisphere facing the thruster. This is generally expressed as the ion current fraction (η_i), i.e., the total ion current over the discharge current.

Knowing the xenon mass flow rate injected in the thruster channel it is also possible to compute how much of the propellant is ionized. The ratio of the ion mass flow rate to the atom mass flow rate is called the mass utilization fraction or the propellant utilization η_{prop}. In the current calculation, we assume that all collected ions are singly charged ions, that means η_{prop} is slightly overestimated. The impact is mainly noticeable at high voltage (>300 V) when the multiply charged ion fractions become relevant. Finally, the divergence of the beam (α_d) is defined as the half-angle of the cone containing 90% of the ion current.

Some test chamber effects can affect the ion current profiles. Most notably, the residual plasma as well as scattering and charge exchange collisions between ions and atoms of the residual gas in the chamber can artificially increase the collected ions current [30], [31]. Those effects are particularly strong at high angles, where the background plasma density can be in the same order as the density of the plasma produced by the thruster. Moreover, the ion current density at high angles, although low, contributes significantly to the total current as they represent a bigger part of the integration hemisphere.

Correction methods can vary from very complex fitting of the experimental profiles to a preexisting plume shape

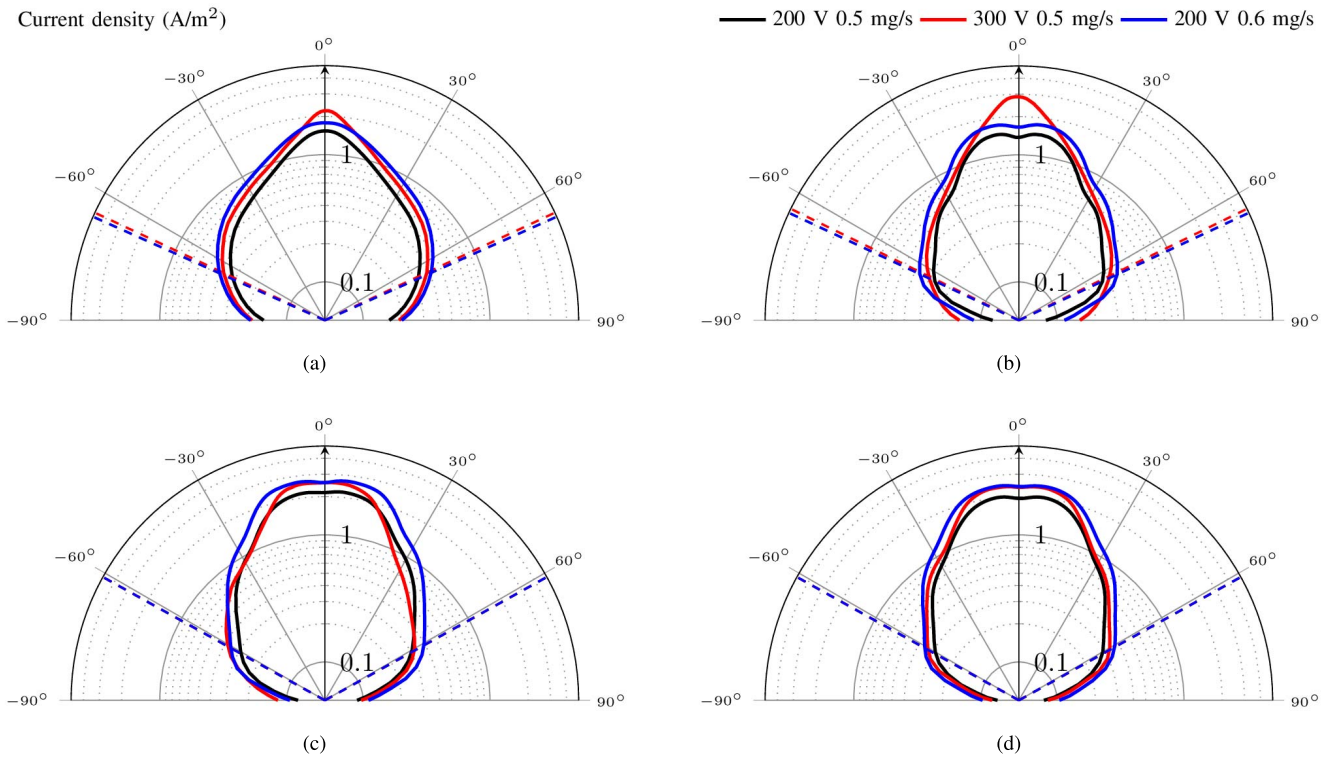

Fig. 4. Current density profiles across the plume of each configurations at 200 V 0.5 mg/s, 300 V 0.5 mg/s, and 200 V 0.6 mg/s operating conditions. The dashed lines represent the computed divergence angle α_d. (a) S_0 B_0. (b) S_0 $2B_0$. (c) $2S_0$ B_0. (d) $2S_0$ $2B_0$.

TABLE I

OVERVIEW OF THE DATA DERIVED FROM PLUME MEASUREMENTS FOR THE 200 V 0.6 mg/s AND 300 V 0.5 mg/s CASES FOR ALL CONFIGURATIONS

			S_0			$\mathbf{2}S_0$		
	V_d (V)	$\dot{m}_a$ (mg/s)	α_d (°)	η_I	η_{prop}	α_d (°)	η_I	η_{prop}
B_0	300	0.5	65	57%	62%	63	63%	77%
	200	0.6	66	53%	59%	61	71%	82%
$\mathbf{2}B_0$	300	0.5	64	69%	60%	62	69%	81%
	200	0.6	65	64%	62%	61	72%	76%

model to very simple background subtraction. Since all the plume data presented in this paper is acquired in the same vacuum chamber with the same measuring instrument, angular profiles and associated quantities can be compared with no additional post processing. We, however, chose to remove the background plasma by subtracting a fixed offset corresponding to the average flux measured at $+90°$ and $-90°$. This ensures that the data are at least somewhat comparable to data from other publications. Comparisons between various sets should be made with great care as chamber effects, probe design, and data processing procedures can greatly influence the numerical results [31].

Table I shows plume data obtained in all four configurations for the 200 V 0.6 mg/s and the 300 V 0.5 mg/s points. Those, respectively, represent a discharge power close to 100 and 140 W for all configurations. From this table, it is apparent that the main parameter that influences the divergence angle is the channel width. The S_0 configurations all have higher divergence than the $2S_0$ ones. Widening the discharge channel also seems to considerably increase the propellant ionization, in agreement with previous studies on a 200 W HT [26]. The ion current fraction (η_I) is also increased with a wider channel but mainly for the high mass flow and low-voltage operating points.

The magnetic field intensity does not greatly influence the plume divergence angle. The loss of one degree of divergence at higher field strength is not very conclusive. While the error bars of such measurement are complicated to estimate, they are almost certainly higher than one degree [31]. The ion beam current fraction shows an increase particularly significant at the highest voltage. This is consistent with the fact that HTs fitted with coils generally increase their magnetic field strength when operating at high voltages in order to maintain a low-discharge current and a large efficiency. Finally, the propellant utilization does not have any clear behavior tied to the magnetic field intensity.

C. Electric Field

The electric field inside a thruster can be measured through laser-induced fluorescence (LIF) spectroscopy. This technique has been extensively used in our research team and details about the optical bench, detection branch, and data treatment are available in the literature [32]. LIF relies on the Doppler

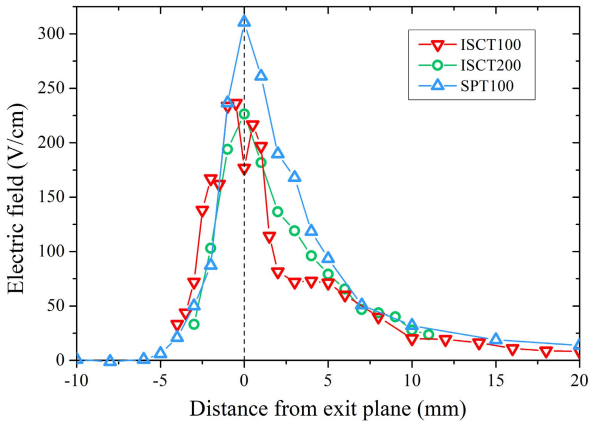

Fig. 5. Electric field measured by LIF at 200 V in the 100-W ISCT100 ($2S_0$ $2B_0$) and the 200-W ISCT200, and at 250 V in the 1.3 kW SPT100.

shift of the absorption spectra of metastable Xe^+ ions. The fluorescence signal collected is proportional in intensity to the density of metastable ions at the velocity probed. Assuming that the ratio of metastable to ground state ions is constant across all velocity groups at a given position, we can reconstruct the ion velocity distribution function (IVDF) at this position.

The most probable ion velocity in the laser beam direction can easily be inferred from the measured IVDF. Assuming a collisionless medium, the velocity profile can be transformed into a potential energy profile, which in turn is used to compute the electric field distribution [33]. The anode potential is usually used as the reference. A second-order centered difference differentiating scheme is used here to derive the electric field. This method was found to be a reasonable approximation when estimating the axial electric field [33].

Measurements of the electric field were performed along the discharge channel centerline from 4 mm inside the discharge channel to 20-mm downstream of the exit plane. Only the best working configuration of $2S_0$ $2B_0$ had its electric field measured. The thruster was operated at 200 V and 0.5 mg/s during the LIF measurements. Fig. 5 shows a comparison between the electric fields of the 100-W thruster used in this paper, of a 200-W HT with a similar $2S_0$ channel configuration operated at 200 V and laboratory model of the 1.5-kW-class SPT100 thruster operated at 250 V. The three thrusters have BN-SiO_2 channel walls. It is interesting to note that across all those sizes, power, and **B** field strength ranges the on-axis electric field profile does not change very much. Accounting for the higher discharge voltage in the case of the SPT100, all of the thrusters have a maximum electric field near the exit plane with a value of about 200 V/cm. The electric field distribution is slightly wider in the downstream region for the larger thrusters. This similarity is a further indication that no matter the size or magnetic field strength, HTs all operate near the same plasma conditions. It is for instance established that the current density is always in the order of 0.1 A/cm^2 for a HT that operates around its normal conditions [11].

The ion axial kinetic energy behind the acceleration region can be inferred from the LIF data. The maximum ion energy is 155, 151, and 211 eV for the ISCT100, ISCT200, and SPT100 HTs, respectively. Those values show energy losses are around 45 eV and they do not depend upon the thruster geometry and magnetic field strength provided that the wall material stays unchanged.

D. Performances

Thrust measurements were performed in the PIVOINE-2G test bench. The facility has been designed for testing thrusters between 1- and 20-kW input power. It consists in a $\varnothing$ 2.2×4 m cylindrical vacuum chamber fit with a 2 00 000 l/s cryogenic pumping system. Since the ISCT100 operates at very low power, and thus, at very low mass flow rates, with respect to what the chamber is designed for, excellent background pressure were achieved. During testing, all measurements were carried out with a residual gas pressure between 4 and 6×10^{-6} mBar-Xe.

The thrust was recorded using a simple pendulum thrust stand. A capacitive sensors with a resolution of 0.2 μm measures the displacement of the moving platform supporting the thruster. The displacement is calibrated against the force exerted by known masses. Calibration is performed with the thruster off right after each test case in order to account for the thermal drift. The resulting thrust measurement has an accuracy in the order of ±0.3 mN. The thrust uncertainty is the single most important contributor to the uncertainty on the specific impulse and the anode efficiency. Only the S_0 $2B_0$ and $2S_0$ $2B_0$ configurations have been investigated as they offer the highest propellant utilization and the lowest divergence angle, see Table I. The S_0 $2B_0$ proved to be even harder to start in the PIVOINE-2G vacuum chamber than in the NExET chamber. This was probably due to the lower background pressure. As a result, only two operating points were measured with the S_0 channel geometry. For the two tested configurations the discharge current was slightly lower in the PIVOINE-2G chamber than in the NExET one, due once again to the lower residual gas pressure, see reference [31].

As can be seen in Fig. 6(a), a thrust between 4 and 9 mN was measured across the tested operating envelop, i.e., between 50 and 250 W. At equivalent mass flow and discharge voltage, the S_0 $2B_0$ configuration both had a lower thrust, a lower specific impulse. and a lower anode efficiency, as can be seen in Fig. 6(a)–(c). The $2S_0$ $2B_0$ configuration achieves a specific impulse I_{sp} between 850 and 1300 s and an anode efficiency η between 25% and 32% for most of the design operating range. The two quantities I_{sp} and η reads:

$$I_{sp} = \frac{T}{\dot{m} g_0} \quad \eta = \frac{T^2}{2\dot{m} U_d I_d}. \tag{1}$$

where T is the thrust, $\dot{m}$ the gas mass flow rate, g_0 is the standard gravity of the Earth, and I_d and U_d the discharge current and applied voltage, respectively. Thrust, Isp, and efficiency increase with mass flow. A significant uncertainty (±3%) is present on the anode efficiency due to the limits in thrust stand sensitivity. The best operating point was reached at 300 V and 0.7 mg/s that corresponds to a discharge power of 180 W: a thrust of 9 mN, an anode specific impulse of 1300 s, and an anode efficiency of 32%.

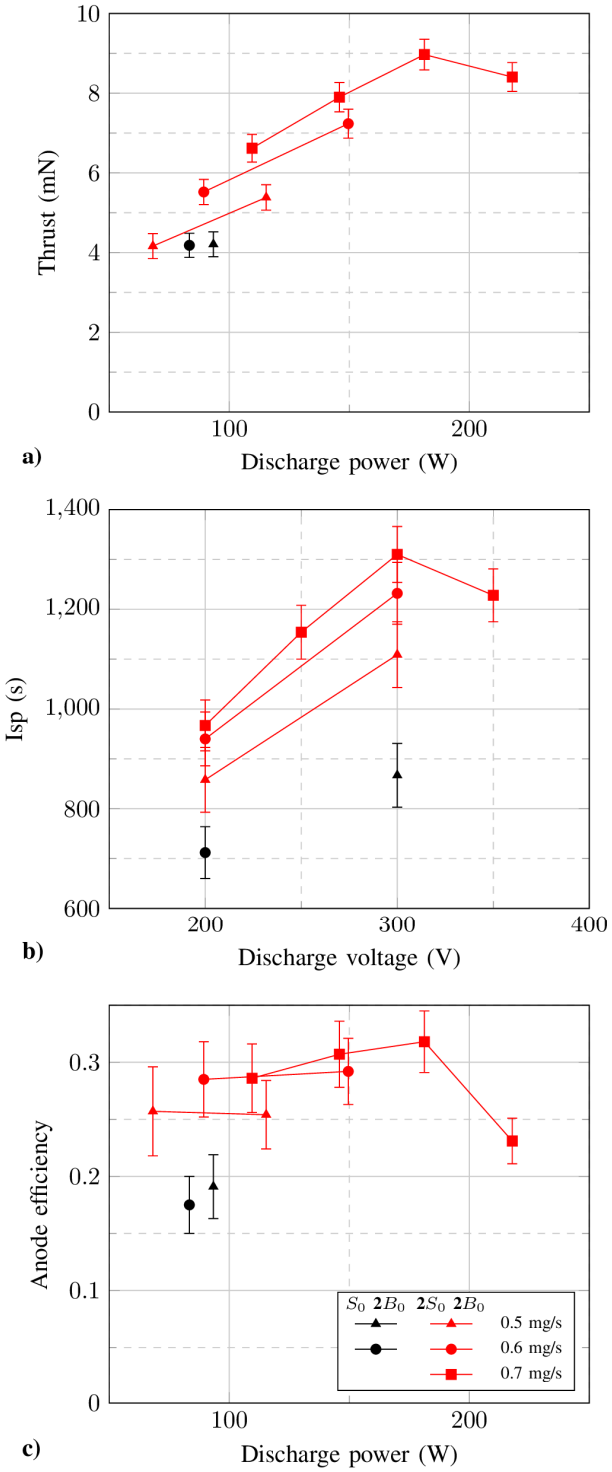

Fig. 6. (a) Thrust versus power for different anode mass flow rates and for two thruster configurations. (b) Anode specific impulse versus voltage. (c) Anode efficiency versus input power.

IV. Comparison With Existing Low-Power Thrusters

Performances of the ISCT100 HT in the $2S_0 2B_0$ configuration are compared with the performances of commercial and laboratory HT with similar sizes and input power in terms of anode efficiency, see Fig. 7. The selected thrusters are,

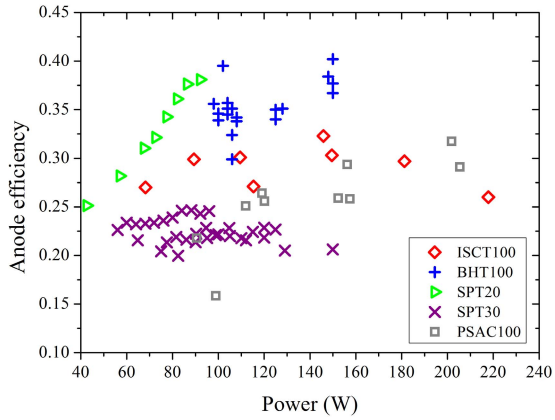

Fig. 7. Comparison of the anode efficiency of 100-W-class low-power HTs (BHT-100 [34], SPT-20 [35], SPT-30 [19], and PSAC 100 [36])

in addition to the ISCT100, the BHT-100 American HT [34], the SPT-20 Ukrainian HT [35], the SPT-30 Russian HT [19], and the PSAC 100 [36] from Singapore. The ISCT100 has a relatively flat performance curve over a wide range of operating conditions, i.e., between 50 and 250 W in comparison with, e.g., the SPT-20 and the SPT-30 thrusters. The performances of the ISCT100 are globally lower by 5% to 8% compared with the BHT-100 and SPT-20. This might be due to the wall material and/or to the magnetic field topology. Our technology readiness level is, however, lower than the one of these two HTs.

V. Conclusion

This paper clearly confirms a HT can operate with xenon around 100-W input power with an efficiency of about 30%, while achieving a thrust-to-power ratio of about 50 mN/kW, close to the one of high power devices. This paper also shows that the electric field distribution along the channel centerline does not depend much on the thruster sizes for a given discharge voltage. This fact suggests that the physical mechanisms that govern the magnetized plasma discharge of a HT are not much affected by sizes and power.

A second version of the ISCT100 HT is currently in preparation. This new version will be optimized in terms of gas injection system, geometry, and magnetic field topology, aiming at higher thrust and anode efficiency around 40%. A dedicated low-current hot cathode will be developed in parallel.

References

[1] T. Wekerle, J. Bezerra Pessoa Filho, L. E. Vergueiro Loures da Costa, and L. Gonzaga Trabasso, "Status and trends of smallsats and their launch vehicles—An up-to-date review," *J. Aerosp. Technol. Manage.*, vol. 9, no. 3, pp. 269–286, 2017.

[2] W. P. Wright and P. Ferrer, "Electric micropropulsion systems," *Prog. Aerosp. Sci.*, vol. 74, pp. 48–61, Apr. 2015.

[3] J. Hudson, S. Spangelo, A. Hine, D. Kolosa, and K. Lemmer, "Mission analysis for Cubesats with micropropulsion," *J. Spacecraft Rockets*, vol. 53, no. 5, pp. 836–846, 2016.

[4] K. Lemmer, "Propulsion for Cubesats," *Acta Astron.*, vol. 134, pp. 231–243, May 2017.

[5] S. Mazouffre, "Electric propulsion for satellites and spacecraft: Established technologies and novel approaches," *Plasma Sources Sci. Technol.*, vol. 25, no. 3, p. 033002, 2016.
[6] M. Keidar *et al.*, "Electric propulsion for small satellites," *Plasma Phys. Controlled Fusion*, vol. 57, no. 1, p. 014005, 2015.
[7] J. Mitterauer, "Micropropulsion for small spacecraft: A new challenge for field effect electric propulsion and microstructured liquid metal ion sources," *Surf. Interface Anal.*, vol. 36, nos. 5–6, pp. 380–386, 2004.
[8] A. Reissner, N. Buldrini, B. Seifert, F. Plesescu, C. Scharlemann, and J. G. del Amo, "mN-FEEP thruster module design and preliminary performance testing," in *Proc. 33rd Int. Electr. Propuls. Conf.*, Washington, DC, USA, 2013, pp. 1–13, paper IEPC 2013-G.
[9] R. S. Legge, Jr., and P. C. Lozano, "Electrospray propulsion based on emitters microfabricated in porous metals," *J. Propuls. Power*, vol. 27, no. 2, pp. 485–495, 2011.
[10] T. Vialis, J. Jarrige, and D. Packan, "Geometry optimization and effect of gas propellant in an electron cyclotron resonance plasma thruster," in *Proc. 35th Int. Electr. Propuls. Conf.*, Atlanta, GA, USA, 2017, pp. 1–12, paper IEPC 2017-378.
[11] D. M. Goebel and I. Katz, *Fundamentals of Electric Propulsion*. Hoboken, NJ, USA: Wiley, 2016.
[12] D. M. Goebel, R. E. Wirz, and I. Katz, "Analytical ion thruster discharge performance model," *J. Propuls. Power*, vol. 23, no. 5, pp. 1055–1067, 2004.
[13] D. Feili *et al.*, "Performance mapping of new μN-RITs at Giessen," in *Proc. 29th Int. Electr. Propuls. Conf.*, Princeton, NJ, USA, 2017, pp. 1–7, paper IEPC 2005-252.
[14] M. Tsay, K. Hohman, N. Rosenblad, E. Ehrbar, M. Robin, and C. Farnell, "Micro radio-frequency ion propulsion system," in *Proc. 48th Joint Propuls. Conf.*, Atlanta, GA, USA, 2012, pp. 1–11, paper AIAA 2012-3947.
[15] J.-P. Boeuf, "Tutorial: Physics and modeling of Hall thrusters," *J. Appl. Phys.*, vol. 121, no. 1, p. 011101, 2017.
[16] V. V. Zhurin, H. R. Kaufman, and R. S. Robinson, "Physics of closed drift thrusters," *Plasma Sources Sci. Technol.*, vol. 8, no. 1, pp. R1–R20, 1999.
[17] S. J. Hall *et al.*, "High-power performance of a 100-kW class nested Hall thruster," in *Proc. 35th Int. Electr. Propuls. Conf.*, Atlanta, GA, USA, 2017, pp. 1–23, paper IEPC 2017-228.
[18] J. Szabo *et al.*, "Performance evaluation of an iodine-vapor Hall thruster," *J. Propuls. Power*, vol. 28, no. 4, pp. 848–857, 2012.
[19] D. T. Jacobson and R. S. Jankovsky, "Test results of a 200 W class Hall thruster," in *Proc. 34th Joint Propuls. Conf.*, Cleveland, OH, USA, 1998, pp. 1–14, paper AIAA 1998-3792.
[20] M. Y. Potapenko, V. V. Gopanchuk, and S. V. Olotin, "PlaS-40 development status: New results," in *Proc. 34th Int. Electr. Propuls. Conf.*, Hyogo-Kobe, Japan, 2015, pp. 1–10, paper IEPC 2015-99.
[21] D. Lev, R. Eytan, G. Alon, A. Warshavsky, and L. Appel, "CAM200 Hall thruster—Development overview," in *Proc. 66th Int. Astron. Congr.*, Jerusalem, Israel, 2015, pp. 1–5, paper IAC 2015-C444.
[22] C. Ducci, S. Oslyak, R. Albertoni, D. Dignani, and M. Andrenucci, "HT100D performance evaluation and endurance test results," in *Proc. 33rd Int. Electr. Propuls. Conf.*, Washington, DC, USA, 2013, pp. 1–9, paper IEPC 2013-140.
[23] S. Lee, H. Kim, J. Kim, Y. Lim, and W. Choe, "High efficiency compact annular Hall thruster with tailored magnetic field," in *Proc. 52nd Joint Propuls. Conf.*, Salt Lake City, UT, USA, 2016, pp. 1–4, paper AIAA 2016-4623.
[24] L. Grimaud, S. Mazouffre, and C. Boniface, "Performance comparison between standard and magnetically shielded 200 W Hall thrusters with BN-SiO_2 and graphite channel walls," in *Proc. 35th Int. Electr. Propuls. Conf.*, Atlanta, GA, USA, 2017, pp. 1–15, paper IEPC 2017-172.
[25] D. Lev *et al.*, "The technological and commercial expansion of electric propulsion in the past 24 years," in *Proc. 35th Int. Electr. Propuls. Conf.*, Atlanta, GA, USA, 2017, pp. 1–18, paper IEPC-2017-242.
[26] S. Mazouffre, G. Bourgeois, K. Dannenmayer, and A. Lejeune, "Ionization and acceleration processes in a small, variable channel width, permanent-magnet Hall thruster," *J. Phys. D: Appl. Phys.*, vol. 45, no. 18, p. 185203, 2012.
[27] K. Dannenmayer and S. Mazouffre, "Elementary scaling relations for Hall effect thrusters," *J. Propuls. Power*, vol. 27, no. 1, pp. 236–245, 2011.
[28] R. Joussot, L. Grimaud, and S. Mazouffre, "Examination of a 5 A-class cathode with a LaB 6 flat disk emitter in the 2 A-20 A current range," *Vacuum*, vol. 146, pp. 52–62, Sep. 2017.
[29] N. Gascon, M. Dudeck, and S. Barral, "Wall material effects in stationary plasma thrusters. I. Parametric studies of an SPT-100," *Phys. Plasmas*, vol. 10, no. 10, pp. 4123–4136, 2003.
[30] D. L. Brown, M. L. R. Walker, J. Szabo, W. Huang, and J. E. Foster, "Recommended practice for use of Faraday probes in electric propulsion testing," *J. Propuls. Power*, vol. 33, no. 3, pp. 582–613, 2017.
[31] S. Mazouffre, G. Largeau, L. Garrigues, C. Boniface, and K. Dannenmayer, "Evaluation of various probe designs for measuring the ion current density in a Hall thruster plume," in *Proc. 35th Int. Electr. Propuls. Conf.*, Atlanta, GA, USA, 2013, pp. 1–17, paper IEPC 2017-336.
[32] S. Mazouffre, "Laser-induced fluorescence diagnostics of the cross-field discharge of Hall thrusters," *Plasma Sources Sci. Technol.*, vol. 22, no. 1, p. 013001, Nov. 2012.
[33] J. Vaudolon and S. Mazouffre, "Indirect determination of the electric field in plasma discharges using laser-induced fluorescence spectroscopy," *Phys. Plasmas*, vol. 21, no. 9, p. 093505, Sep. 2014.
[34] J. J. Szabo, R. Tedrake, E. Metivier, S. Paintal, and Z. Taillefer, "Characterization of a one hundred Watt, long lifetime Hall effect thruster for small spacecraft," in *Proc. 53rd Joint Propuls. Conf.*, Atlanta, GA, USA, 2017, pp. 1–15, paper AIAA 2017-4728.
[35] A. V. Loyan and T. A. Maksymenko, "Performance investigation of SPT-20 M low power Hall effect thruster," in *Proc. 30th Int. Electr. Propuls. Conf.*, Florence, Italy, 2007, pp. 1–14, paper IEPC 2007–100.
[36] J. W. M. Lim *et al.*, "Automated integrated robotic systems for diagnostics and test of electric and μ-propulsion thrusters," *IEEE Trans. Plasma Sci.*, to be published.

Stéphane Mazouffre received the master's degree in material science and plasma physics from The Limoges Computer Sciences Engineering School, University of Limoges, Limoges, France, in 1996, and the Ph.D. degree in the field of low-temperature plasma physics from the University of Eindhoven, Eindhoven, The Netherlands, in 2001.

He is currently a Research Director with the French Science Center (CNRS), Orléans, France. He is also the Head of the Electric Propulsion Team, ICARE laboratory in Orléans. He has authored over 80 scientific publications and 115 conference papers. His current research interests include Hall thrusters and variants, new concepts of electrical thrusters, the physics of magnetized discharges and laser-aided diagnostics for electric propulsion.

Dr. Mazouffre is a member of the American Institute of Aeronautics and Astronautics and the Board of Directors of the Electrical Rocket Propulsion Society. He was a recipient of the Bronze Medal of the CNRS in 2008 and the Noah Hershkowitz Award of the Institute of Physics in 2012.

Lou Grimaud received the M.S. degree in aerospace engineering from ENSMA, France, and the Illinois Institute of Technology, Chicago, IL, USA, in 2014. He is currently pursuing the Ph.D. degree with the Electric Propulsion Team, ICARE CNRS Laboratory, Orléans, France, under the supervision of Dr. S. Mazouffre.

His current research interests include low erosion Hall thrusters, such as magnetic shielding and wall less, low power Hall thrusters, and plasma diagnostics.